Bioactive Materials 20 (2023) 29–40

Contents lists available at ScienceDirect

Bioactive Materials

journal homepage: www.keaipublishing.com/en/journals/bioactive-materials

Nano-calcium silicate mineralized fish scale scaffolds for enhancing tendon-bone healing

Fei Han [a,1], Tian Li [a,b,1], Mengmeng Li [a], Bingjun Zhang [a], Yufeng Wang [c], Yufang Zhu [a,b,**], Chengtie Wu [a,b,*]

[a] State Key Laboratory of High-Performance Ceramics and Superfine Microstructure, Shanghai Institute of Ceramics, Chinese Academy of Sciences, Shanghai, 200050, PR China
[b] Center of Materials Science and Optoelectronics Engineering, University of Chinese Academy of Sciences, Beijing, 100049, PR China
[c] Department of Orthopaedic Surgery, Nanjing First Hospital, Nanjing Medical University, Nanjing, 210006, PR China

ARTICLE INFO

Keywords:
Fish scales
Tendon repair
High strength
Bioactivities
Tendon-bone healing enhancement

ABSTRACT

Tendon-bone healing is essential for an effective rotator cuff tendon repair surgery, however, this remains a significant challenge due to the lack of biomaterials with high strength and bioactivity. Inspired by the high-performance exoskeleton of natural organisms, we set out to apply natural fish scale (FS) modified by calcium silicate nanoparticles (CS NPs) as a new biomaterial (CS-FS) to overcome the challenge. Benefit from its "Bouligand" microstructure, such FS-based scaffold maintained excellent tensile strength (125.05 MPa) and toughness (14.16 MJ/m^3), which are 1.93 and 2.72 times that of natural tendon respectively, allowing it to well meet the requirements for rotator cuff tendon repair. Additionally, CS-FS showed diverse bioactivities by stimulating the differentiation and phenotypic maintenance of multiple types of cells participated into the composition of tendon-bone junction, (e.g. bone marrow mesenchymal stem cells (BMSCs), chondrocyte, and tendon stem/progenitor cells (TSPCs)). In both rat and rabbit rotator cuff tear (RCT) models, CS-FS played a key role in the tendon-bone interface regeneration and biomechanical function, which may be achieved by activating BMP-2/Smad/Runx2 pathway in BMSCs. Therefore, natural fish scale -based biomaterials are the promising candidate for clinical tendon repair due to their outstanding strength and bioactivity.

1. Introduction

Natural tendons/ligaments are noted for their excellent tensile strength and toughness, which are connected to the bone via mineralized/unmineralized fibrocartilage layers (enthesis tissue) and transmit forces between bones and between bone and muscle. However, tendon/ligament injury occurs very frequently in the clinic, and the reconstruction of the tendon-bone interface is a critical process within many types of tendon repair surgeries [1–3]. Due to the long rehabilitation period, strain dependence scarring and poor vascularization, the post-operative restore native tendon bone interface (enthesis tissue) remains a great challenge [4,5]. Over the past several decades, implantation of tendon grafts/patches has been proposed to be an effective strategy for promoting healing of injured tendons and reconstructed tendon-bone interface, as well as restoring the motor function of patients. However, current tendon implantation materials are suboptimal: most tendon substitutes fail to both provide excellent mechanical support and exert good bioactivity [6,7]. For instance, artificial ligaments made of non-degradable polymers, such as polyethylene terephthalate (PET)--based ligament augmentation and reconstruction system (LARS®), Dacron and Gore–Tex, possess excellent mechanical performances [8,9]. However, these scaffolds displayed unsatisfactory bioactivity to enable appropriate new tissue ingrowth and host tissue integration, which result in poor tendon-bone interface healing, and even complications

Peer review under responsibility of KeAi Communications Co., Ltd.

* Corresponding author. State Key Laboratory of High-Performance Ceramics and Superfine Microstructure, Shanghai Institute of Ceramics, Chinese Academy of Sciences, 1295 Dingxi Road, Shanghai, 200050, PR China.
** Corresponding author. State Key Laboratory of High-Performance Ceramics and Superfine Microstructure, Shanghai Institute of Ceramics, Chinese Academy of Sciences, 1295 Dingxi Road, Shanghai, 200050, PR China.
E-mail addresses: zhuyufang@mail.sic.ac.cn (Y. Zhu), chengtiewu@mail.sic.ac.cn (C. Wu).
[1] These authors contributed equally to this work.

https://doi.org/10.1016/j.bioactmat.2022.04.030
Received 8 January 2022; Received in revised form 14 April 2022; Accepted 26 April 2022

such as synovitis and long-term implant rupture [10–12]. Other strategies, such as allografts and autografts, preserve the structure and components of natural tendons, as well as bioactive molecules. However, negative effects, such as donor site morbidity, adverse immune responses and synovitis, lead to a high surgical failure rate and limit the clinical application of these strategies [6,13,14]. Current strategies based on biological means for enhancing tendon-bone interface regeneration consist mainly of applying bioactive materials, suitable seed-cells/stem cells, growth factors, and gene delivery, alone or in combination, to the reconstructed interface [15,16]. To date, few of these alternatives has provided a successful long-term solution. First of all, the tensile strength of the bioactive materials is a significant property that should not be overlooked as a healthy tendon tissue is naturally under tension. Recently, researchers have attempted to develop new fibrous scaffolds for tendon repair based on electrospinning or wet-spinning technology, and accelerated tendon-bone healing by adding bioactive substances, such as magnesium and lithium ions, to the nanofibers [17–20]. Unfortunately, the tensile strength of most reported fibrous scaffolds failed to match that of natural tendon [7]. Secondly, the utilization of growth factors or stem cell delivery to enhance tendon bone healing is also a strategy of great interest [15,16]. Despite it presented positive effects on the regeneration of enthesis, a number of potential problems cannot be ignored. The existing stem cell therapies have limitations such as limited in vitro expansion efficiency, source and rejection reactions, tumorigenicity and ethical concerns [15,16]. What's more, the high cost and potential risk of growth factors also limit their application [21]. Therefore, the novel engineered tendon substitutes with excellent biocompatibility, bioactivity and mechanical properties that are capable of accelerating native tendon-bone interface regeneration are urgently needed for the clinical treatment of tendon injury.

Intriguingly, after aeons of evolution, many organisms have developed tissues or organs with special hierarchical microstructures. The most typical example is fish scale (FS), which has a "Bouligand" microstructure consisting of lamellae of collagen fibrils with different orientations that is similar to a revolving staircase. Such microstructure provides excellent mechanical properties through the synergistic effect of deformation mechanisms, including collagen fibril delamination, rotation, stretching and sliding [22,23]. These mechanisms endow FS with astounding toughness and elasticity under tensile load stress (Fig. S1). Coincidentally, the main components of natural FS are collagen and a small amount of hydroxyapatite (HA) [24,25], which are similar to the matrix components of bone and tendon, as marine organisms-derived collagen has been proved to possess good biocompatibility and low immunogenicity compared with terrestrial organisms-derived collagen [26], thus, FS may be a potential option for tendon tissue engineering. However, the bioactivity of natural FS may be limited, as its microstructure remained long-term stabilization in liquid environment [22]. which means its inner mineralized layer will not release calcium and phosphate ions to regulate the tissue repair microenvironment. Therefore, the objective of this research is to propose strategies for preparation of "bioactivated" FS, that is, conferring it with both excellent bioactivity and mechanical properties which are indispensable for design of high-performance rotator cuff substitutes.

It has been demonstrated that inorganic ions are essential for normal anabolic function of tissue and tissue-specific cell function [7,27,28], which also enlightens us. Herein, we propose an innovative "bioactivation strategy" to prepare a calcium silicate-"bioactivated" fish scale (CS-FS) scaffold through the mineralization of CS NPs uniformly on collagen fibers *in situ* via a vacuum-induced biomineralization method. Although calcium phosphate (CaP) is the major inorganic content of enthesis matrix, calcium silicate (CS)-based bioactive materials have been proved to possess better biodegradability and osteogenic activity compared with CaP-based biomaterials (hydroxyapatite, β-TCP, etc.) [29,30]. Moreover, CS exhibited the capability for promoting the regeneration of varieties of tissues by releasing silicon and calcium ions [31–34]. Therefore, we propose the hypothesis that CS deposited on FS will performs as an "bioactivating factor" to "bioactivate" FS and thus confer it with the ability to repair different organs and transitional tissues. In this study, the microstructure and mechanical properties of CS-FS were evaluated, to ensure that CS-FS still maintains the mechanical properties which is superior to reported biodegradable tendon scaffolds and allowing it to meet the requirements for tendon repair. Moreover, *In vitro* experiments were presented to confirm the capability of silicon and calcium ions for accelerating the regeneration of tendon, bone and the tendon-bone interface, so as to verify the bioactivity of CS-FS scaffolds. Finally, the therapeutic effects of the CS-FS scaffolds in repairing tendon injuries and promoting tendon-bone interface healing were demonstrated in both rat and rabbit rotator cuff tear (RCT) models, and the biomechanical properties of the regenerated tissue were further evaluated.

2. Results and discussion

2.1. Concepts of the framework for CS-FS fabrication via a vacuum-induced biomineralization method

FS is a potential candidate for tendon tissue engineering due to its excellent mechanical properties. It has been reported that natural FS possesses a multilayered spiral lamellar structure, i.e., a "Bouligand" structure, on the microscale level, which is conducive to the dispersion of stress [22,23]. CS is a widely used bioactive material that can directly promote the regeneration of varieties of tissues (bone [31], cartilage [32,33], adipose tissue [34], myocardium [35], etc.) by releasing silicon and calcium ions; thus, it was chosen as an "bioactivating factor" to "bioactivate" FS and thus confer it with the ability to repair different organs and transitional tissues. As shown in Fig. 1, in this study, the stable mineralized layer (containing HA deposition) of natural FS was removed firstly. Then, the FS were placed in a vacuum environment with calcium salt solution dripped on its surface. With the assistance of vacuum, calcium ions could enter the gap between the FS collagen fibers, so that the calcium ions were fully combined with carbonyl and carboxyl groups on collagen fibers as mineralization sites for CS mineralization. Subsequently, silicate ions entered into the gap of collagen fibers under the vacuum condition, and combined with the calcium ions on collagen to form CS. This method of in-situ CS mineralization in FS was named vacuum-induced biomineralization method. By adjusting the concentration of calcium salt and silicate salt in the solution, FS scaffolds mineralized with different amounts of CS were obtained. The CS-FS scaffold was cut into a square tendon patch of appropriate size to repair rotator cuff injury in rat and rabbit models. Both ends of the CS-FS scaffold connected the teared tendon stump and humeral head and sustained tensile force at the interface, while by releasing silicon and calcium ions, CS-FS scaffold would promote the healing of tendon defect and tendon bone interface.

2.2. Morphology, microstructure and mechanical properties of CS-FS

By observing the cross-sectional morphology of FS scaffolds, it was confirmed that all kinds of FS scaffolds maintained a "Bouligand" spiral microstructure. Compared with the 0FS and 0.2CS-FS groups, the 0.5CS-FS, 0.75CS-FS and 1CS-FS groups showed a large number of inorganic particles deposited in the collagen interlayers. The results of mapping analysis also confirmed that the composition of the deposition was CS (Fig. S2). Firstly, after decalcification treatment of natural FS (0FS), no phosphorus and calcium elements were detected in 0FS, that is, the originally stable mineralized layer was completely removed. Subsequently, Ca^{2+} and SiO_3^{2-} entered the interlayer during the vacuum-induced mineralization process and combined to form CS NPs (Fig. S2). Additionally, a certain amount of mineralization deposition was also observed on the surface of each fish scale scaffold (Fig. S3). As shown in Fig. 2, 0FS was composed of a large number of collagen fiber bundles, and from 0FS group to 1CS-FS group, it can be observed that the

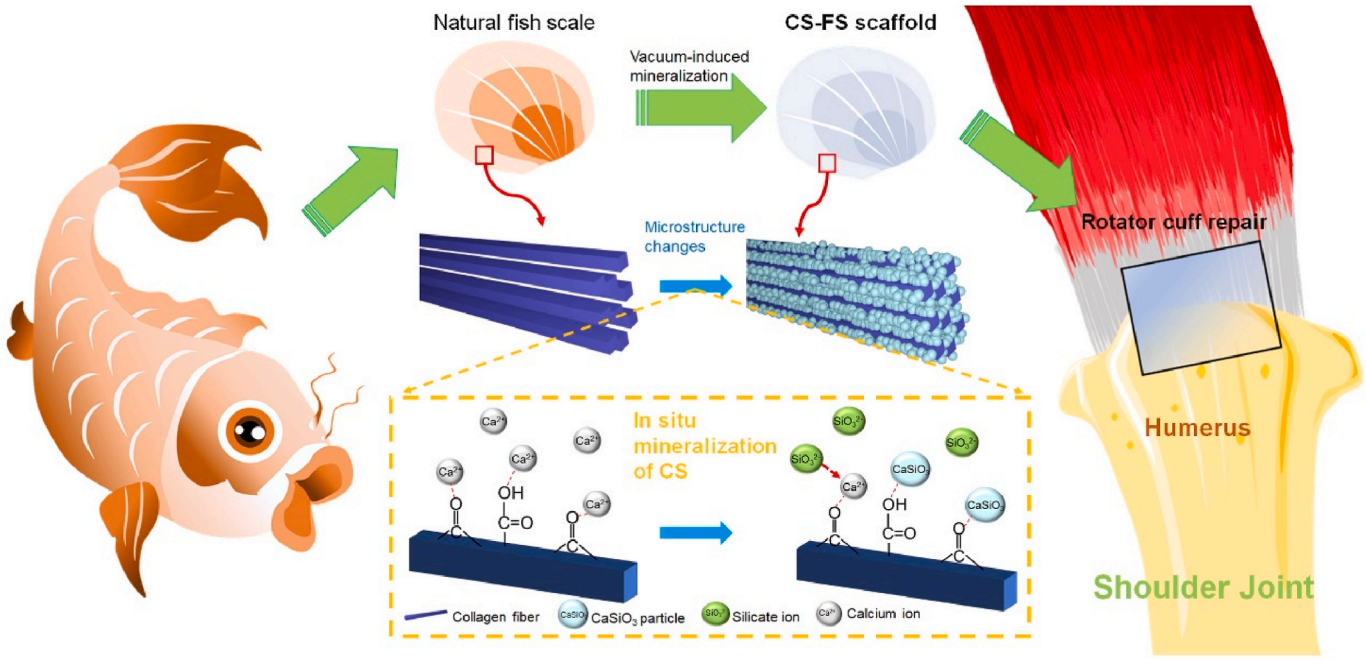

Fig. 1. Schematic summarizing work on the fabrication of calcium silicate (CS)-"bioactivated" fish scale scaffold (CS-FS) by vacuum-induced mineralization, for tendon defect repair. In the vacuum-induced mineralization process, Ca^{2+} ions can engage in coordinating chelation interactions with the carbonyl and carboxyl groups of collagen fibers in fish scale and subsequently combined with SiO_3^{2-} ions to induce the *in situ* formation of CS particle. The silicon and calcium ions released from CS-FS contributed to the regeneration of tendon-bone interface and the healing of tendon defect.

inorganic particles in the interlayer gradually increase, while the collagen fiber bundles became illegible. In particular, in the 1CS-FS group, the deposition of inorganic particles between the interlayers was most obvious, even when the collagen fiber bundle was completely wrapped. The interaction between FS collagen fiber and deposited CS NPs was further explored by high-resolution transmission electron microscopy (HRTEM) analysis. In Fig. 2G, the HRTEM image clearly shows that dense inorganic particles with a diameter of 40.43 ± 9.51 nm were bound to the surface of collagen fibers and evenly wrapped around the collagen fibers. Electron diffraction pattern and energy spectrum analysis by HRTEM also confirmed that the particles were amorphous CS NPs (Fig. 2H). Previous studies reported that Ca^{2+} ions can engage in coordinating chelation interactions with the carbonyl and carboxyl groups of collagen fibers and then became the nucleation sites of nano-hydroxyapatite [36,37]. As a consequence, it is reasonable to speculate that during the process of vacuum-induced mineralization, FS collagen fibers act as templates for Ca^{2+} ions through coordination with their carboxyl groups and subsequently induce the *in-situ* formation of CS NPs. In addition, as shown in Supplementary Fig. S4A, the results of thermogravimetric analysis (TGA) showed that the content of CS in the CS-FS scaffolds increased from 0.2CS-FS to 1CS-FS. Subsequent inorganic ion release tests also confirmed that the concentrations of released Ca^{2+} and SiO_3^{2-} ions was related to the content of CS in CS-FS scaffolds (Supplementary Figs. S4B–C). Interestingly, the "activated" CS-FS scaffolds showed controlled ion release behavior. On the first day of release, there was an initial burst of Ca^{2+} and SiO_3^{2-} ion release in all groups, and subsequent sustained release of ions was detected for up to 14 days. The inorganic ions released from CS-FS scaffolds may improve the biological properties of FS and enhance the effect of FS in promoting tissue repair.

As ideal implantation biomaterials for clinical tendon repair, CS-FS scaffolds should possess excellent mechanical properties to bear the tension between muscle and bone. In this study, the mechanical properties of CS-FS scaffolds in each group were investigated through tensile-strain measurements. As shown in Fig. 3, the maximum tensile strength, toughness, stain at failure and Young's modulus of 0FS, that is, FS after decalcification treatment, were not decreased compared with those of natural FS (Original Fish Scale, O-FS), especially when its maximum tensile strength was as high as 125.05 ± 7.24 MPa(The toughness, Young's modulus and Strain at failure of 0FS group are also similar to that of O-FS group, 0FS: 14.16 ± 2.67 MJ/m^3, 664.62 ± 67.81 MPa, 18.06 ± 3.07%; O-FS: 11.23 ± 2.04 MJ/m^3, 717.73 ± 47.92 MPa, 14.38 ± 1.98%) This result indicates that the loss of the mineralized layer of natural FS had little effect on its mechanical properties. Although the average tensile strength, toughness and Young's modulus of 0.2CS-FS and 0.5CS-FS were decreased (Table 1), there was no significant difference between 0.2CS-FS or 0.5CS-FS and 0FS. The tensile strength and toughness of these three groups were higher than those of the natural tendon. While there was no significant difference in the Strain at failure between the three groups and values were close to that of the natural tendon (Table 1). However, from 0.75CS-FS to 1CS-FS, the mechanical properties of FS decreased significantly with increasing calcium silicate deposition. One possible reason for this phenomenon is that a high concentration of silicate solution causes a strongly alkaline environment, which hydrolyses some collagen fibers during the vacuum-induced mineralization process, resulting in degeneration of the "Bouligand" structure. The "Bouligand" layer of FS plays a significant role in dissipating stress when it bears external tension [22]. It is composed of multiple sublayers of aligned collagen fiber bundles arranged into a spiral pattern. The direction of each pair of adjacent sublayers is different, and they rotate at a certain angle. When FS is under tension, the collagen fiber bundles parallel to the tension direction can be stretched and deformed until interlaminar separation occurs. Other collagen fiber bundles at a certain angle to the tensile direction can twist along the tensile direction and deform to disperse the tensile force. In addition, the interlayer displacement can further disperse the tensile force. In general, exactly as shown in Fig. 3F and Table S1, the mechanical properties of CS-FS prepared in this study are significantly better than most of the reported biodegradable tendon repair scaffolds, which is exhilarating.

Moreover, in contrast with natural tendons, CS-FS scaffolds exhibit better toughness and tensile strength, implying that the mechanical properties of CS-FS scaffolds can meet the requirements for tendon

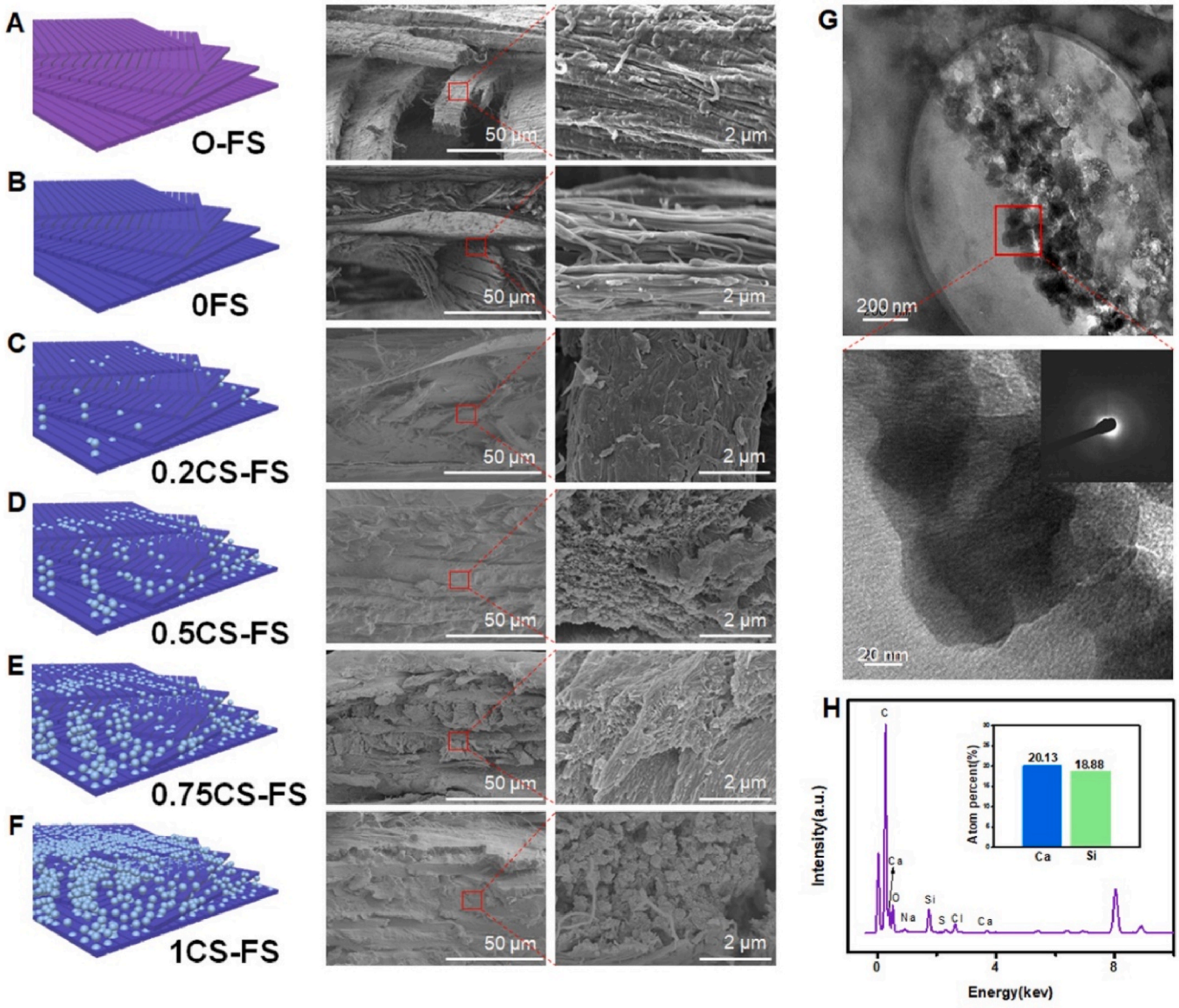

Fig. 2. Microstructure and morphology of CS-FS scaffolds with different CS mineralization level. (A to F) Scanning electron microscope (SEM) images presented the internal microstructure and different mineralization levels of CS-FS scaffolds in each group. In addition, the attached schematic diagram shows the structure changes of each group. (G) High-resolution transmission electron microscopy (HRTEM) images showed the pattern of the deposited CS produced by vacuum-induced mineralization on the FS collagen fibers. The CS particles which are evenly distributed along the collagen fibers were observed. (H) Energy spectrum analysis confirmed that the particles observed in HRTEM images were CS.

implantation, bearing tension between muscle and bone. Of special interest, CS-FS scaffolds and natural tendons exhibit similar Young's moduli, which may prevent the potential negative influence of stress shielding on tendon healing. Previous studies confirmed that, the high-strength suture will lead to stress shielding and acellular area in repaired tendon [39], which is more unfavorable for tendon healing. Although there is little research on the effect of stress shielding caused by tendon grafts on tendon repair, generally, this is an interesting finding, but further research is needed.

2.3. Effect of CS-FS on cell viability and differentiation

At present, there seems to be an absence of research on the biocompatibility of FS-derived bioscaffolds. To evaluate the bioactivity of CS-FS scaffolds, cell proliferation, adhesion and differentiation were investigated. In this study, bone marrow mesenchymal stem cells (BMSCs), chondrocytes and tendon stem/progenitor cells (TSPCs) were utilized as models of the cell types at the natural tendon-bone interface and to explore the effect of CS-FS scaffolds on tendon-bone healing. Chondrocytes used in this work were derived from the cartilage of rabbit knee joint and simply served as a cell model due to the specific markers expressed in chondrocytes and fibrocartilage are consistent. As illustrated in Supplementary Fig. S5, cell proliferation increased with culture time in all groups, while cells cultured with 0.75CS-FS and 1CS-FS groups showed reduced cell proliferation, which may have been related to the excessive release of silicon and calcium ions. It seems that exorbitant concentrations of calcium and silicon ions inhibit cell proliferation. Regarding cell adhesion and morphology, all cells exhibited excellent dispersion and adhesion as well as a stretched flat morphology and plenty of pseudopodia after 24 h of seeding on scaffolds in each group. These results demonstrated that CS-FS scaffolds have excellent biocompatibility for supporting cell adhesion and growth on the surface and are promising candidate tissue engineering scaffolds.

Furthermore, the expression of differentiation markers was measure

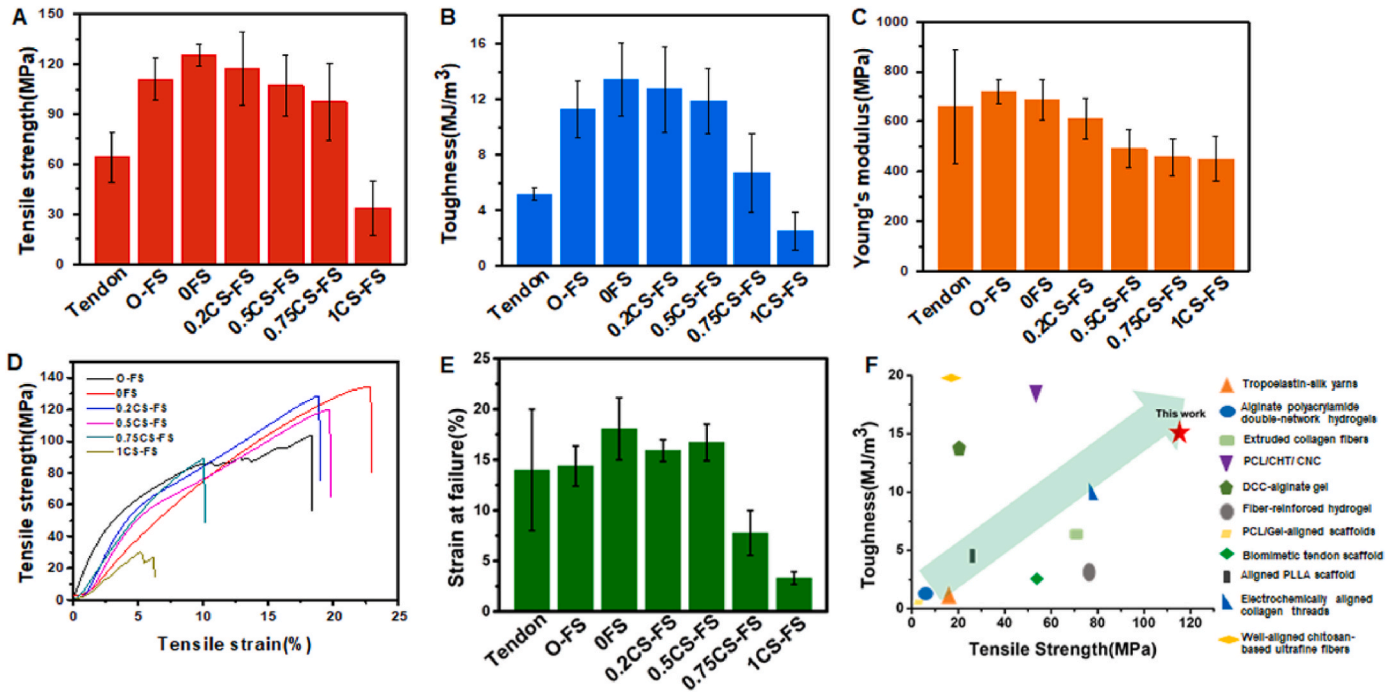

Fig. 3. Mechanical properties of CS-FS scaffolds. Comparison of (A) maximum tensile strength, (B) Toughness, and (C) Young's modulus of untreated FS (O-FS), different CS-FS scaffolds and natural tendon. (The data of natural tendons obtained from previously reported study [38].) Tensile stress-strain curves (D) and Strain at failure (E) of O-FS and each CS-FS scaffold. (F) Ashby diagram of toughness and young's modulus for reported tendon tissue engineering scaffolds [63–74]. This indicates that the mechanical strength of CS-FS scaffolds with a certain amount of mineralization is completely suitable for tendon repair.

Table 1
The mechanical performances of nano-calcium silicate mineralized fish scale scaffolds.

	Tensile strength (Mpa)	Load to failure (N)	Thickness (mm)	Toughness (MJ/m^3)	Young's modulus (Mpa)	Stain at failure (%)
O-FS	110.85 ± 12.51	146.53 ± 11.2	0.30 ± 0.03	11.23 ± 2.04	717.73 ± 47.92	14.38 ± 1.98
0FS	125.05 ± 7.24	142.82 ± 40.33	0.25 ± 0.06	14.16 ± 2.67	664.62 ± 67.81	18.06 ± 3.07
0.2CS-FS	116.97 ± 22.10	127.68 ± 13.90	0.23 ± 0.02	12.69 ± 3.05	609.46 ± 80.37	15.91 ± 1.07
0.5CS-FS	107.36 ± 18.25	133.31 ± 19.13	0.26 ± 0.04	11.89 ± 2.34	489.98 ± 75.88	16.71 ± 1.80
0.75CS-FS	91.60 ± 18.55	93.74 ± 27.15	0.21 ± 0.03	6.71 ± 2.81	455.36 ± 78.59	7.76 ± 2.21
1CS-FS	33.55 ± 16.36	40.21 ± 13.97	0.33 ± 0.06	2.50 ± 1.36	417.73 ± 78.06	3.31 ± 0.62
Natural tendon [38]	64.7 ± 15	NA	NA	5.175 ± 0.4	660 ± 266	14 ± 6

to verify the capability of CS-FS scaffolds to promote cell differentiation. As shown in Fig. 4, the scaffolds with higher CS content (0.5CS-FS, 0.75CS-FS, 1CS-FS) significantly promoted the expression of osteogenic differentiation-related genes (Runx2, Opn, Ocn and Col1) in rabbit BMSCs. These three scaffolds also showed stronger Osteopontin (Opn) fluorescence, indicating higher intracellular Opn protein levels. Consistent with previous studies, silicon ions and calcium ions are capable of promoting osteogenic differentiation of BMSCs at a certain concentration [40–42]. Additionally, the 0.2CS-FS and 0.5CS-FS groups showed higher expression levels of chondrocytes phenotype -related genes (Sox9, Agreecan, and N-cadh) and stronger N-cadh protein fluorescence, which is also consistent with previous studies; that is, silicon and calcium ions are capable of maintaining chondrocytes phenotype of chondrocytes [32,33]. Interestingly, silicon and calcium ions released by CS-FS scaffolds also had an effect on the differentiation of TSPCs. TSPCs cultured on 0.5CS-FS showed relatively higher expression of Tnc, Bgn and Col 1 than those cultured on the other scaffolds, while TSPCs cultured on 0.75CS-FS showed higher expression of Bgn and Col 1 than those cultured on the other scaffolds. Furthermore, cells cultured on both of these scaffolds showed stronger Col 1 protein fluorescence than those cultured on the other scaffolds. It seems that silicon and calcium ions can also play an important role in the differentiation of TSPCs and tendon regeneration. At present, only a few studies have confirmed the beneficial effect of silicon and calcium ions on tendon repair [28,43], but the specific mechanism by which ions promote tendon regeneration is still unclear and needs to be further explored.

Specifically, 0.5CS-FS showed excellent bioactivity in all cell types; thus, in the follow-up experiments, 0.5CS-FS was selected to verify the biological function of CS-FS scaffolds. Next, with the aim of simulating the cellular composition of the surgically reconstructed tendon-bone interface, where the tendon is riveted to the humeral head (bone surface), we designed a BMSC and TSPC co-culture system based on Transwell to explore the potential role of CS-FS scaffolds in tendon-bone healing. There were three co-culture groups with different BMSC/TSPC ratios (1:2, 1:1, 2:1, the total number of cells was kept the same), and BMSCs or TSPCs cultured alone on CS-FS scaffolds served as controls (the scaffolds selected for the co-culture system were 0FS and 0.5CS-FS, The groups in which cells were cultured alone on 0FS or 0.5CS-FS scaffolds were set as controls, namely, S0 and S0.5. In the co-culture system, the group of cells cultured on 0FS was named C0, and the group of cells cultured on 0.5CS-FS scaffolds was named C0.5). Then, the expression of osteogenic and tenogenic differentiation-related genes was evaluated by Q-PCR 3 days after cell seeding. As shown in Fig. S6, the C0.5 group exhibited the highest gene expression levels of Runx2, Opn and Ocn, especially at a BMSC/TSPC ratio of 2:1, indicating that CS was capable of accelerating the osteogenic differentiation and mineralization of BMSCs at the tendon-bone interface. In addition, in the C0.5 group, CS promoted the expression of the Smad1, Smad5 and BMP-2

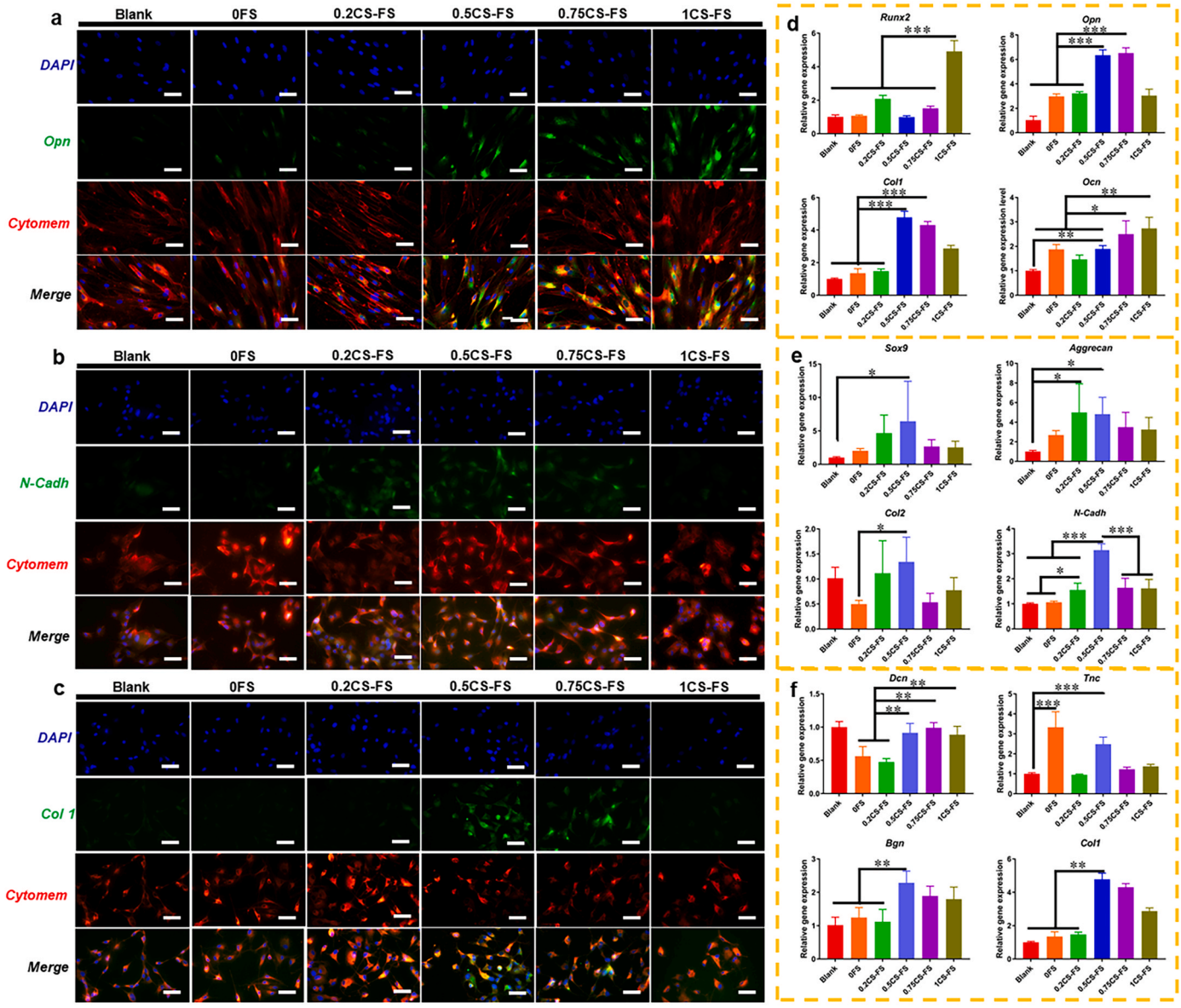

Fig. 4. The CLSM images of the specific markers and Q-PCR analysis of specific gene expression for BMSCs, Chondrocytes and TSPCs cultured on CS-FS scaffolds in each group. The CLSM images showed the fluorescence labelled (A) Opn in BMSCs, (B) N-cadh in Chondrocytes and (C) Col 1 in TSPCs. Bar 100 μm (D) Expression of osteogenic differentiation-related genes in BMSCs cultured on each CS-FS scaffold. (E) Expression of chondrocytes phenotype-related genes in Chondrocytes cultured on each CS-FS scaffold. (F) Expression of tenogenic differentiation-related genes in TSPCs cultured on each CS-FS scaffold. CS deposition improved the bioactivity of FS scaffolds which promoted cell differentiation of several tissue cells.

genes in BMSCs in co-culture system (Fig. S7). As previous studies have confirmed that Ca–Si bioceramics can activate the Smad-dependent BMP signaling pathway, inducing the accumulation of phosphorylated-Smad1/5 in osteoblasts nucleus and the activation of the BMP downstream cascade (OCN, OPN and Runx2) [44,45], this data implied that the CS in FS scaffold may activated the BMP-2/Smad/Runx2 signaling pathway in co-cultured BMSCs to further promote osteogenic differentiation. However, in the co-culture systems with BMSC/TSPC ratios of 1:1 and 2:1, the expression of genes related to tenogenic differentiation (Dcn, Col 1, and Bgn) in TSPCs was decreased. In the co-culture system with a BMSC/TSPC ratio of 1:1, the Sox9 gene, which is related to chondrogenic differentiation, showed high expression.

2.4. Restorative effect of CS-FS on tendon related injury in vivo

In clinical RCT repair, the restoration of the fibrocartilage layer and tendon quality are crucial for enhancing the biomechanical properties of the tendon postoperatively. The natural tendon-bone interface, that is, the insertion point (enthesis), comprises transitional tissue composed of layered fibrocartilage tissue, which ensures that the tendon is firmly fixed on the bone and allows transmission of stress [46]. It is necessary to reconstruct the tendon-bone interface once the tendon is injured in many clinical cases, but the regenerated interface is often composed of scar tissue with poor biomechanical properties [47]. On the other hand, affected by many negative factors, such as aging and stress shielding caused by suture, the quality of patients' tendon is always poor, which may lead to tendon re-tear [48]. Therefore, in this study, two RCT models were utilized to investigate the therapeutic effect of CS-FS scaffolds in tendon injury repair: a rat RCT model and a rabbit RCT model. Moreover, a widely accepted material for tendon grafts in the clinic, namely, PET ligaments (LARS®), was used as one of the control groups. As 0.5CS-FS not only maintained excellent mechanical properties, but also showed positive bioactivity for various cells, we selected 0.5CS-FS for subsequent experiments to verify its role in improving

tendon-bone healing *in vivo*. As shown in Fig. S10, in the rat RCT model, the 0FS and 0.5CS-FS scaffolds showed partial degradation and absorption at 8 weeks postoperatively with almost no inflammatory cell infiltration or fat infiltration. The results of safranin red o/fast green staining demonstrated that more fibrocartilage was stained red at the tendon-bone interface in the 0.5CS-FS group than in the other groups. The quantitative analysis also confirmed this; the relative area of fibrocartilage in the 0.5CS-FS group was significantly larger than that in the other three groups. Less fibrocartilage and more loose fibrous tissue and fat infiltration was observed at the graft-bone interface in the PET group than in the 0CS-FS group and 0.5 CS-FS group, which was attributed to the biological inertia of the PET. H&E staining and Masson's staining revealed that, although the blank group and 0FS group also presented a tight connection between tendon tissue and bone tissue, as in the 0.5CS-FS group, the 0.5CS-FS group showed some aligned fibrocartilage tissue and a small number of mature chondrocytes at the tendon-bone interface. Therefore, at 8 weeks postoperatively, the histopathological score of the 0.5CS-FS group was significantly higher than

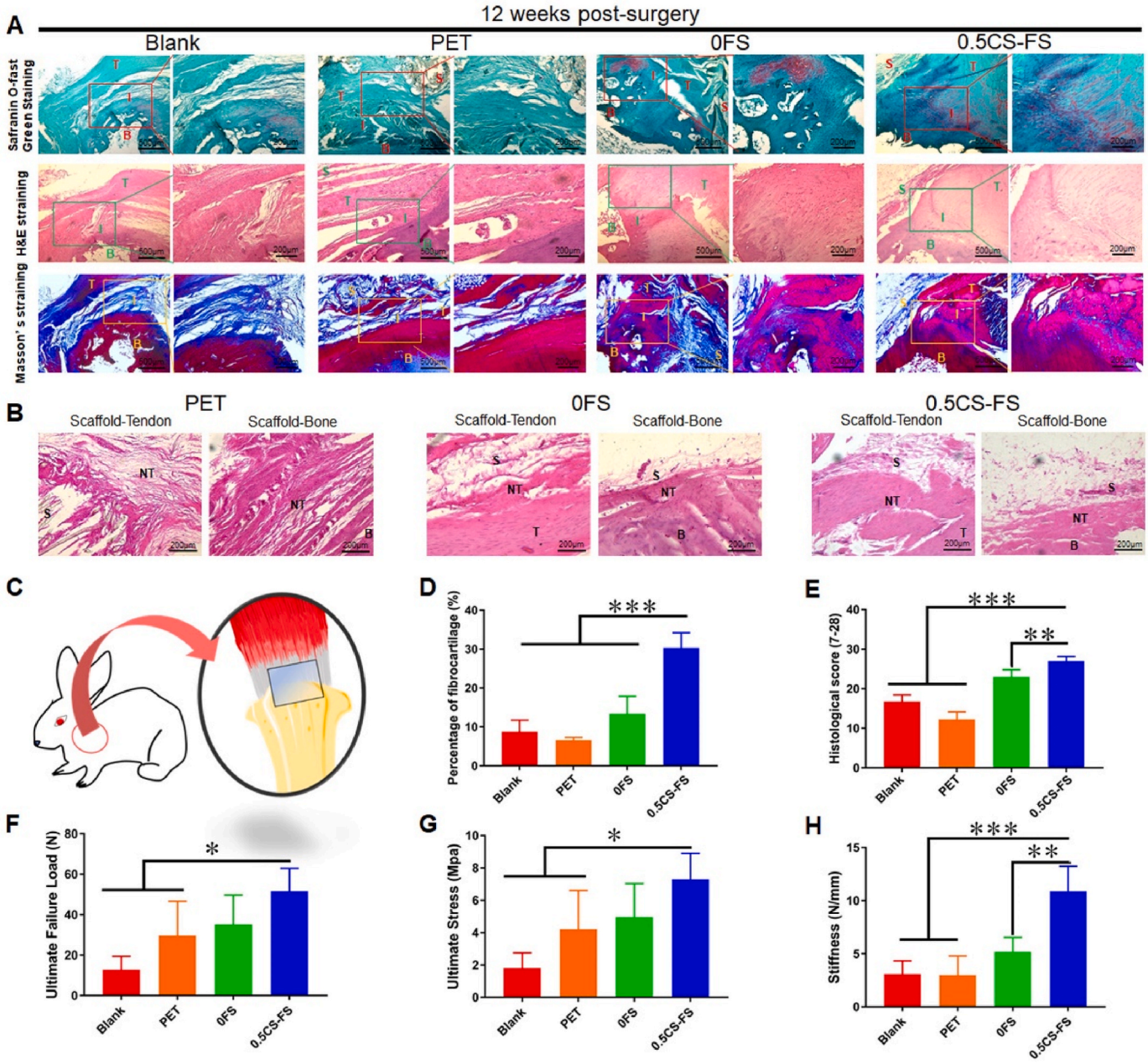

Fig. 5. Histopathological analysis and biomechanical analysis of the therapeutic effect of CS-FS scaffolds on RCT in rabbit models. (A) The images of safranin-o-fast green staining, H&E staining and Masson' s staining showed the healing of tendon-bone interface and the regeneration of fibrocartilage in each group 12 weeks after surgery. (B) The images of H&E staining illustrated the integration of each scaffolds with injured host tendon stump and host bone, and the growth of new tendon tissue and new bone tissue between scaffold and host tissue. 'T' in the figures represents the host tendon, that is, the injured host tendon stump; 'B' refers to the host bone; 'I' identifies the tendon-bone interface; 'S' represents the scaffold; 'NT' refers to new tendon tissue or bone tissue between scaffold and host tissue. (C) A brief schematic diagram of the RCT repair using CS-FS in rabbit models. (D) Quantitative analysis of the relative area of fibrocartilage tissue at the regenerated tendon-bone interface which was executed based on the images of safranin-o-fast green staining. (E) Histological score, the scoring rules followed previous studies and 4 colleagues performed a double-blind scoring. (F to H) Biomechanical analysis of repaired rotator cuff tendon in each group 12 weeks after surgery. The detection items are (F) Ultimate failure load, (G) Ultimate stress and (H) stiffness. n = 4, *P < 0.05, **P < 0.01, ***P < 0.001.

that of the other three groups (Fig. S10E). In addition, the joint between scaffold and host tendon stump, as well as the joint between scaffold and host bone were treated with H&E staining. As shown in Fig. S10B, this result illustrated that 0.5CS-FS could promote the growth of aligned new tendon tissue at host tendon stump compared with PET and 0FS scaffold. Although the maturity of new tissue was lower than that of host tendon, it was a favorably phenomenon for the improvement of the quality of injured tendon, Moreover, the integration of scaffold and bone presented to be equally good, a small amount of new bone tissue and bone vortex structure were observed. Correspondingly, in the PET group, the interface between the PET scaffold and host tissue was fulfilled with a large amount of disorderly fibrous tissue, and fat infiltration was also observed which was considered as a sign of degenerative change in tendon disease [49].

A similar tendency was observed in the rabbit RCT model. As shown in Fig. 5, new fibrocartilage tissue was much less abundant in the 0.5CS-FS group than in the rat model group, but a complete fibrocartilage layer had also regenerated. In contrast, in the blank group and 0FS group, a small amount of fibrocartilage tissue rather than a relatively complete fibrocartilage layer had regenerated in some areas. More importantly, 0.5CS-FS scaffold promoted the growth of new tendon tissue and new bone tissue at the junction of scaffold and host tissue. In the failure mode analysis, 12 weeks after the operation, the ultimate failure load of the 0.5CS-FS group (51.65 ± 11.34 N) was significantly higher than that of the PET and blank groups, while there was no significant difference between the 0.5CS-FS group and the 0FS group (Fig. 5F–G). The ultimate stress of the 0.5CS-FS group was 7.30 ± 1.60 MPa, which was significantly higher than that of the other three groups. In addition, the stiffness of the 0.5CS-FS group (10.88 ± 2.37 N/mm) was significantly higher than that of the PET group and blank group, but there was no significant difference between the 0.5CS-FS group and the 0FS group. Although the biomechanical properties of the CS-FS group are still not equivalent to those of a normal rabbit rotator cuff, it is noteworthy that the 0.5CS-FS group has reached 73.2% of ultimate failure load of a normal rotator cuff (51.65 ± 11.34 N vs. 70.6 ± 8.6 N [50]). Meanwhile, the 0.5CS-FS group has reached 55.3% of stiffness of a normal rotator cuff. (10.88 ± 2.37 N/mm vs. 19.7 ± 3.3 N/mm [50]). Compared to the other three groups, the biomechanical properties are much closer to those of a normal tissue. In general, the rotator cuffs repaired with 0.5CS-FS presented better biomechanical properties than those repaired with the other materials.

Taking inspiration from the ECM composition of natural tendon-bone interface, most previous researches have focused on incorporating inorganic biomaterials (e.g. CaP) and/or biodegradable organic biomaterials into specific regions of a scaffold to mimic the structure of non-mineralized and mineralized fibrocartilage in enthesis for enhancing tendon-bone healing [51,52]. Recently, there have been a number of promising new advances and strategies for the enhancement of tendon-bone healing. For example, novel decellularised matrix scaffolds with a special structure have shown the advantage of improved enthesis regeneration [52,53]. Some researchers proposed a book-shaped acellular scaffold by sectioning the natural fibrocartilage to fabricate a book-shaped decellularised matrix scaffold, which displayed an excellent capability of cell delivery and inducibility of fibrocartilage formation [54,55]. Structural modification of scaffolds and thus influencing cell behaviour by topographical cues and improving regeneration of enthesis is also an emerging strategy [51,52]. The niche-mimicking features of physical topographic cues have been confirmed to have a significant effect on cellular behavior and tissue formation [56]. For instance, Samavedi et al. fabricated an aligned-to-random electrospinning scaffold using offset spinnerets which could direct the specific cell morphology to promote tendon-bone healing [57]. Other promising technologies, such as 3D-printing scaffolds and scaffold-based multicellular co-culture systems [58–60], have also performed favorably in promoting tendon-bone healing *in vivo* or in vitro. However, as we mentioned above, few biodegradable scaffolds are equipped with the similar mechanical properties as natural tendon, which means that if the scaffold ruptures after implantation due to its inability to withstand tension, it is likely to result in undesirable interface regeneration or even surgical failure. After aeons of evolution, some natural materials presented outstanding mechanical properties due to their hierarchical microstructure. Based on this, the study offers new insight that, to utilize this characteristic of natural materials to prepare high-performance biomaterials for tissue or organ repair. Just like the fish scales-based biomaterial introduced in this paper exhibits mechanical properties superior to those of natural tendon. More importantly, in combination with the above in vitro results, it can be concluded that the released silicate and calcium ions from CS-FS promoted the *in-situ* differentiation of stem cells and phenotype maintenance in the short term, as well as accelerating the process of tendon-bone healing and inhibiting the formation of fibrous scar tissue in a long-term *in vivo* experiment. Finally, these results mean that CS-FS provided solutions to solve the problem that have been bothering clinicians, that is, how to improve the quality of injured rotator cuff tendon and how to promote tendon-bone healing, which also reflecting the advantages of CS-FS as a tendon substitute.

3. Conclusion

In this work, fish scales were selected to transform into biomaterials for tendon repair and successfully solved the issue of insufficient mechanical strength of tendon repair scaffolds. On the other hand, after modified by CS NPs, CS-FS exhibited diverse bioactivities, for multiple types of cells derived from bone-interface-tendon, BMSCs, chondrocyte, and TSPCs, and CS-FS was capable of significantly stimulating cell differentiation and phenotypic maintenance. Most importantly, CS-FS promoted the repair of rotator cuff tendon and transitional tissue between tendon and bone *in vivo*, indicating that the inorganic ions, that is, the combination of Ca and Si ions produced a more positive integrated effect on facilitating the repair of bone-interface-tendon. The study suggests that the combination of natural fish scales and bioactive ions represents a new class of high-performance biomaterials to repair complex tissues.

4. Materials and methods

4.1. Preparation of the CS-FS scaffold

Firstly, the scales were selected from the larger scales of black carp (mylopharyngodon piceus, the diameter of scales was 2~3 cm), and cleaned with plenty of running water. Their epidermis, fascia and other soft tissue were removed using forceps and scalpel. After the cleaning was completed, the scales of black carps were immersed in a 75% ethanol solution (AR, Sinopharm Chemical Reagent Co., Ltd., Shanghai, China) and treated under ultrasound for 10 min to kill any pathogenic microorganisms that might be present inside the scales. Then the cleaned FSs was immersed in ethylene diamine tetra acetic acid decalcification solution (EDTA, 10%, pH = 7.2, Solarbio, Beijing, China) decalcifying solution for one week to remove the natural mineralized layer in FS. After washing with deionized water, the decalcified FSs were dried in an oven at 60 °C for 10 min and then placed at room temperature for standby, named as 0FS. The composition of the decalcified fish scales will be examined by scanning electron microscopy (SEM, SU8220, Hitachi, Japan) analysis and Mapping analysis. Subsequently, FS scaffolds for in-situ mineralization of CS were fabricated. 0FS samples were divided into five groups, four of which were treated with different concentrations of calcium nitrate solution and sodium silicate solution respectively. The concentrations of calcium nitrate solution and sodium silicate solution used in each group were the same. Beforehand, $Na_2SiO_3 \cdot 9H_2O$ and $Ca(NO_3)_2 \cdot 4H_2O$ (AR, Sinopharm Chemical Reagent Co., Ltd., Shanghai, China) were dissolved in deionized water respectively, and different concentrations of Na_2SiO_3 solution (0.2 M, 0.5 M, 0.75 M and 1 M) and $Ca(NO_3)_2$ solution (0.2 M, 0.5 M, 0.75 M and 1 M)

were prepared. The dried 0FS samples were soaked in 50 ml $Ca(NO_3)_2$ solution of different concentrations (0.2 m, 0.5 m, 0.75 m and 1 m), and then the beakers were placed in a vacuum drying oven which maintained vacuum for 4 h. After freeze-drying, each sample were spread on a culture dish, and 500 μl Na_2SiO_3 solution with different concentrations (0.2 M, 0.5 M, 0.75 M and 1 M) were dripped on the surface of each sample. The dish was then in a vacuum drying oven which maintained vacuum for 4 h to deposit CS *in situ*. Finally, the samples were dried in an oven at 60 °C to obtain FS scaffolds with CS deposition, which were named as 0.2CS-FS, 0.5CS-FS, 0.75CS-FS and 1CS-FS, respectively.

4.2. Characterization

Microstructure of FS scaffolds: Scanning electron microscopy (SEM, SU8220, Hitachi, Japan) was utilized to observe the microstructure of natural FS and CS-FS scaffolds under different magnifications, and the elements in each sample were analysed by energy dispersive spectrometry (EDS). To investigate the binding of calcium silicate (CS) and collagen fibers in CS-FS scaffolds, 1CS-FS scaffolds were embedded in resin, sliced, and then observed by using a high-resolution transmission electron microscope (HRTEM, Tecnai G2 F20, FEI Electron Optics, the Netherlands).

Thermogravimetric analysis: The amount of CS mineralized in CS-FS scaffolds was analysed by thermogravimetric analyzer (TGA, STA409PC, Netzsch, Germany).

Release kinetics of ions: Then, the release kinetics of calcium and silicon ions from CS-FS scaffolds was measured by plasma atomic emission spectroscopy (ICP, 715-ES, Varian, USA). In short, CS-FS scaffolds from each group were cut into 1-cm-diameter discs and immersed in a centrifuge tube filled with 10 ml deionized water ($n = 4$). The centrifuge tubes were placed on a shaker at a constant temperature of 37 °C, and the liquid was removed at different time points for ICP analysis to generate release profiles of silicon and calcium ions.

Mechanical testing: The tensile strength of the FS scaffolds was measured by a universal mechanical testing machine (Instron-5566, Instron, Canton, USA). Maximum load of the loading cell is 10 kN with precision of 0.0001 N (Model 5566, Instron, Canton, MA). Stress-strain curves were collected by Fast-Track software (Instron, Canton, USA). Briefly, all samples ($n > 5$) were cut into dog-bone-shape, with a total length of 24 mm, a width of 5 mm. Both ends of the sample were rectangles with a size of 5 mm × 7 mm, while the length of the middle part was 10 mm and the narrowest width was 2 mm. Further, the ends of the sample were clamped with pneumatic clamps in the dry state. Samples were preconditioned 5 times with 0.5 N of preload and then were loaded to completely broken at a rate of 10 mm/min (strain rate of 1.7%/s). The load and displacement of each patch were recorded at a sample rate of 20 Hz. Stress-strain curves, maximum tensile strength and stress for each group of samples were recorded during the test. The toughness of each FS scaffold and natural FS were calculated according to eq (1) [61]:

$$U = \int_0^{\sigma_f} \sigma \, d\varepsilon \tag{1}$$

where U is the energy per volume absorbed, σ is the stress, ε is the stain, σ_f is the stain of failure.

4.3. In vitro cytocompatibility

Rabbit bone marrow mesenchymal stem cells (BMSCs) and rabbit chondrocytes (Chondrocytes) were purchased from Cyagen Biotechnology Co., Ltd. According to a previous report, primary rabbit tendon stem/progenitor cells (TSPCs) were extracted from rabbit tendon tissue as previous study [62]. BMSCs, Chondrocytes and TSPCs were cultured in complete Dulbecco's modified Eagle's medium (DMEM, Gibco, USA) (Containing 10% fetal bovine serum (FBS, Gibco, USA), 1% IU/ml penicillin and 1 μG/ml streptomycin (Hyclone, USA)) in a humidified incubator (37 °C, 5% CO_2). FS scaffolds from each group were cut into discs 0.8 cm in diameter, soaked in 75% ethanol for 30 min and pasted on the bottom of the wells of a 48-well plate (Corning, USA). The cells were seeded on the scaffolds at a density of 10×10^4 per well. After 24 h, cell adhesion was observed by SEM, and the cytoskeleton of cells from each group was labelled with an F-actin cytoskeleton kit (Alexa Fluor™ 488, Invitrogen, USA). To assess the cell proliferation of different kinds of cells on the FS scaffolds, the cells were seeded on the scaffolds at a density of 2×10^3 per well, and a CCK-8 kit (Dojindo, Japan) was used to analyze the viability of the cells 1, 4 and 7 days after seeding.

4.4. In vitro cell differentiation

To investigate the bioactivity of CS-FS scaffolds in inducing the differentiation of BMSCs, Chondrocytes and TSPCs, Q-PCR and fluorescent labelling of specific proteins were performed. According to the cell culture method described above, FS scaffolds from each group were cut into discs 0.8 cm in diameter and pasted on the bottoms of the wells of a 48-well plate. Then, BMSCs, Chondrocytes and TSPCs were seeded on the samples. After 3 days of culture, the cells were digested with 0.25% trypsin solution, and then mRNA was extracted by using TRIzol reagent (Invitrogen, USA) according to the manufacturer's instructions. The extracted mRNA was reverse transcribed into cDNA with a kit (PrimeScript™ RT reagent Kit, Takara, Japan), and then RT-PCR was performed with a TB green kit according to the manufacturer's instructions (TB Green® Premix Ex Taq™, Takara, Japan) ($n = 4$). In this study, we measured the relative gene expression levels of the osteogenic differentiation-related genes Runx2, Ocn, Opn and Col 1 in BMSCs; the chondrogenic differentiation-related genes Sox9, Aggrecan, Col 2 and N-cadh in Chondrocytes; and the tenogenic differentiation-related genes Dcn, Tnc, Bgn and Col 1 in TSPCs. The related primer sequence information is shown in Table S2. Additionally, three days after the cells were seeded, they were fixed with 4% paraformaldehyde solution. Specific proteins, such as Opn in BMSCs (Antibody purchased from Invitrogen, 24H5L3), N-cadh in Chondrocytes (Antibody purchased from Abcam, ab19348) and Col 1 in TSPCs (Antibody purchased from Abcam, ab19348), were fluorescently labelled, and the fluorescence intensity was observed by laser confocal microscopy.

Next, with the aim of simulating the cellular composition of the surgically reconstructed tendon-bone interface, where the tendon is riveted to the humeral head (bone surface), we designed a BMSC and TSPC co-culture system based on Transwell (Corning, USA) to explore the potential role of CS-FS scaffolds in tendon-bone healing. Based on the above experiments, 0FS and 0.5CS-FS scaffolds were selected to establish the co-culture system. Briefly, BMSCs and TSPCs were seeded on FS samples in a 48-well culture plate following the method described above. After 24 h, the scaffolds were transferred to a Transwell plate. The scaffolds cultured with TSPCs were placed in the upper chamber of a Transwell 24-well plate, while the scaffolds cultured with BMSCs were placed in the bottom chamber. The BMSCs and TSPCs were seeded at three ratios, 1:2, 1:1 and 2:1, and the total number of cells was 10×10^4. After 3 days of culture, the expression of genes related to osteogenic differentiation and tenogenic differentiation in cells was measured by Q-PCR. The groups in which cells were cultured alone on 0FS or 0.5CS-FS scaffolds were set as controls, namely, S0 and S0.5. In the co-culture system, the group of cells cultured on 0FS was named C0, and the group of cells cultured on 0.5CS-FS scaffolds was named C0.5.

4.5. Animal model of rotator cuff injury

This animal study was reviewed and approved by Institutional Animal Care and Use Committee of Nanjing First Hospital, Nanjing Medical University (No. DW201801). All procedures and postoperative care protocols were performed strictly in accordance with the Animal Use and Care Guide. The procedure used to model rotator cuff tear (RCT) and

repair in rabbits is shown in Fig. S8. In short, 20 mature male New Zealand white rabbits (3.0 ± 0.5 kg) were used. The rabbits were and fixed in the supine position under general anaesthesia, the shaved on both shoulders was shaved, and the skin was exposed and disinfected, the supraspinatus tendons of both shoulders were damaged and repaired using scaffolds. Briefly, the skin was cut at the humeral head to expose the rotator cuff tissue, especially the supraspinatus tendon. Next, the supraspinatus tendon was separated by using a sharp Kirschner wire (2.5 mm, Jinzhong Co., Ltd, Shanghai, China). An incision was made at the insertion of the supraspinatus tendon with a scalpel, resulting in a partial RCT. FS scaffolds and PET were cut into 0.8 cm × 1.5 cm pieces. (The PET samples were obtained from the residual waste of LARS® artificial ligament) One end of each scaffold was sutured to the stump of the supraspinatus tendon, and the other end was fixed to the humeral head. Beforehand, a scalpel was used to scrape the area where the humeral head contacted the scaffold to make the clean the interface. A 2.5-mm wide hole was drilled in the humeral head so that a suture could pass through the hole to fix the scaffold, and then the scaffold and tendon stump were firmly attached to the humeral head. After that, the wound was closed and disinfected again. 4-0 Ethibond sutures were used in the surgery (Johnson & Johnson). The rabbits were kept in large cages and allowed to move freely to prevent joint stiffness postoperatively. After 12 weeks, the rabbits were sacrificed. The healing of the tendon-bone interface was investigated by histopathological analysis, and the biomechanical properties of the regenerated rotator cuff were assessed by biomechanical tests. The procedure used to model rat RCT and repair, which is the same as that used for the rabbits, is demonstrated in Fig. S8. Briefly, 12 mature male SD rats (260 ± 22 g) were used in this study. After the rats were anaesthetized and the skin was shaved and disinfected, the supraspinatus tendons of both shoulders were damaged and repaired using scaffolds. The size of each scaffold was 0.3 cm × 0.6 cm. Twelve weeks postoperatively, the rats were sacrificed, and the healing of the tendon-bone interface was investigated by histopathological analysis.

4.6. Histopathological analysis

Twelve weeks postoperatively, the rabbits and rats were sacrificed. The supraspinatus tendon to the humeral head was harvested, and other soft tissues were removed from the humeral head. Next, all the specimens were fixed in 10% neutral formalin solution for 3 days and then immersed in EDTA decalcification solution (Sangon Biotech, Shanghai, China) for 1 month. The completely decalcified specimens were dehydrated in gradient alcohol solutions (30%–100%). After being treated with xylene, the specimens were embedded in paraffin and sectioned along the tendon-to-bone direction at a thickness of 5 μm. Safranine-O-fast green staining, H&E staining and Masson's staining were used to stain the sections according to the manufacturer's instructions (Solarbio Life Science, Beijing, China). The stained sections were observed with a light microscope (eclipse 80i, Nikon), and histopathological images were taken with a camera (ds-5m, Nikon). Then, according to the results of safranine-O-fast green staining, the proportion of fibrocartilage tissue in the tendon-bone interface was calculated with ImageJ software. Additionally, the histological score of each group was determined [63]; the details of the modified histological score system applicated for evaluating of the regenerated tendon-bone interface are listed in Table S3.

4.7. Biomechanical test

All biomechanical tests were carried out with a material testing system (Instron-5566, USA). A total of 4 rabbit supraspinatus brachii tendon specimens from each group were used. The upper limb bone and supraspinatus muscle were retained on the specimens used for biomechanical testing to allow them to be easily clamping, and other soft tissues were removed. To reduce slippage, the humeral head and upper limb bone were fixed in a mould with a diameter of 1.5 cm and denture powder. The supraspinatus tendon was sutured with medical gauze and sandpaper to increase friction, and then the specimen was fixed (Fig. S9). After applying a preload of 1 N with a test speed of 5 mm/min (strain rate of 0.8%/s), the rotator cuff specimen underwent preconditioning for a total of 20 cycles. The ultimate failure load (N), ultimate failure force (MPa) and load deformation curve were recorded. The stiffness (N/mm) of each sample was calculated from the slope of the linear region of the load-deformation curve at the maximal load-to-failure point.

4.8. Statistics

Statistical analysis was conducted in IBM SPSS Statistics 22 software. Data are presented as the mean with standard deviation (s.d.). To determine whether there were any statistically significant differences between the means of independent groups, ANOVA was used for multiple group comparisons and LSD test were used to assess statistical differences.

Ethical approval statement

We further confirm that any aspect of the work covered in this manuscript that involving experimental animals has been conducted with the ethical approval of Institutional Animal Care and Use Committee of Nanjing First Hospital, Nanjing Medical University (approval No. DW201801) and that such approvals are acknowledged within the manuscript.

Declaration of competing interest

Conflicts of interestnone.

CRediT authorship contribution statement

Fei Han: Conceptualization, Methodology, Validation, Formal analysis, Software, Writing – original draft, Visualization. **Tian Li:** Conceptualization, Methodology, Investigation, Validation, Software, Formal analysis. **Mengmeng Li:** Methodology, Validation. **Bingjun Zhang:** Investigation, Validation. **Yufeng Wang:** Methodology, Validation. **Yufang Zhu:** Writing – review & editing, Supervision, Project administration. **Chengtie Wu:** Writing – review & editing, Supervision, Project administration, Funding acquisition.

Acknowledgments

The work was supported by the National Basic Research Program of China (grant No. 2021YFA0715700), the Natural Science Foundation of China (32130062), Innovation Cross Team of Chinese Academy of Sciences (JCTD-2018-13), Science and Technology Commission of Shanghai Municipality (20442420300, 21DZ1205600).

Appendix A. Supplementary data

Supplementary data to this article can be found online at https://doi.org/10.1016/j.bioactmat.2022.04.030.

References

[1] K.E. Aagaard, F. Abu-Zidan, K. Lunsjo, High incidence of acute full-thickness rotator cuff tears A population-based prospective study in a Swedish Community, Acta Orthop. 86 (5) (2015) 558–562, https://doi.org/10.3109/17453674.2015.1022433.

[2] I. Lantto, J. Heikkinen, T. Flinkkila, P. Ohtonen, J. Leppilahti, Epidemiology of Achilles tendon ruptures: increasing incidence over a 33-year period, Scand. J. Med. Sci. Sports 25 (1) (2015) E133–E138, https://doi.org/10.1111/sms.12253.

[3] B. Moses, J. Orchard, J. Orchard, Systematic review: annual incidence of ACL injury and surgery in various populations, Res. Sports Med. 20 (3–4) (2012) 157–179, https://doi.org/10.1080/15438627.2012.680633.

[4] P. Sharma, N. Maffulli, Current concepts review tendon injury and tendinopathy: healing and repair, J. Bone Joint Surg.-Am. 87A (1) (2005) 187–202, https://doi.org/10.2106/JBJS.D.01850.

[5] J.R. Rudzki, R.S. Adler, R.F. Warren, W.R. Kadrmas, N. Vermc, A.D. Pearle, S. Lyman, S. Fealy, Contrast-enhanced ultrasound characterization of the vascularity of the rotator cuff tendon: age- and activity-related changes in the intact asymptomatic rotator cuff, J. Shoulder Elbow Surg. 17 (1) (2008) 96S–100S, https://doi.org/10.1016/j.jse.2007.07.004.

[6] J.M. Chen, J.K. Xu, A.L. Wang, M.H. Zheng, Scaffolds for tendon and ligament repair: review of the efficacy of commercial products, Expet Rev. Med. Dev. 6 (1) (2009) 61–73, https://doi.org/10.1586/17434440.6.1.61.

[7] Y.J. No, M. Castilho, Y. Ramaswamy, H. Zreiqat, Role of biomaterials and controlled architecture on tendon/ligament repair and regeneration, Adv. Mater. 32 (18) (2020), 1904511, https://doi.org/10.1002/adma.201904511.

[8] R. Glousman, C. Shields, R. Kerlan, F. Jobe, S. Lombardo, L. Yocum, J. Tibone, R. Gambardella, Gore-tex prosthetic ligament in anterior cruciate deficient knees, Am. J. Sports Med. 16 (4) (1988) 321–326, https://doi.org/10.1177/036354658801600402.

[9] K. Gao, S.Y. Chen, L.D. Wang, W.G. Zhang, Y.F. Kang, Q.R. Dong, H.B. Zhou, L. A. Li, Anterior cruciate ligament reconstruction with LARS artificial ligament: a multicenter study with 3-to 5-year follow-up, Arthroscopy 26 (4) (2010) 515–523, https://doi.org/10.1016/j.arthro.2010.02.001.

[10] H. Li, Z.J. Yao, J. Jiang, Y.H. Hua, J.W. Chen, Y.X. Li, K. Gao, S.Y. Chen, Biologic failure of a Ligament Advanced Reinforcement System artificial ligament in anterior cruciate ligament reconstruction: a report of serious knee synovitis, Arthroscopy 28 (4) (2012) 583–586, https://doi.org/10.1016/j.arthro.2011.12.008.

[11] T.M. Tiefenboeck, E. Thurmaier, M.M. Tiefenboeck, R.C. Ostermann, J. Joestl, M. Winnisch, M. Schurz, S. Hajdu, M. Hofbauer, Clinical and functional outcome after anterior cruciate ligament. reconstruction using the LARS (TM) system at a minimum follow-up of 10 years, Knee 22 (6) (2015) 565–568, https://doi.org/10.1016/j.knee.2015.06.003.

[12] J.C. Richmond, C.J. Manseau, R. Patz, O. McConville, Anterior cruciate reconstruction using a dacron ligament prosthesis - a long-term study, Am. J. Sports Med. 20 (1) (1992) 24–28, https://doi.org/10.1177/036354659202000107.

[13] J.R. Walton, N.K. Bowman, Y. Khatib, J. Linklater, G.A.C. Murrell, Restore orthobiologic implant: not recommended for augmentation of rotator cuff repairs, J. Bone Joint Surg.-Am. 89A (4) (2007) 786–791, https://doi.org/10.2106/JBJS.F.00315.

[14] S.P. Badhe, T.M. Lawrence, F.D. Smith, P.G. Lunn, An assessment of porcine dermal xenograft as an augmentation graft in the treatment of extensive rotator cuff tears, J, Shoulder Elbow Surg. 17 (1) (2008) 35S–39S, https://doi.org/10.1016/j.jse.2007.08.005.

[15] D. Docheva, S.A. Muller, M. Majewski, C.H. Evans, Biologics for tendon repair, Adv. Drug Deliv. Rev. 84 (2015) 222–239, https://doi.org/10.1016/j.addr.2014.11.015.

[16] S.F. Tellado, E.R. Balmayor, M. Van Griensven, Strategies to engineer tendon/ligament-to-bone interface: biomaterials, cells and growth factors, Adv. Drug Deliv. Rev. 94 (2015) 126–140, https://doi.org/10.1016/j.addr.2015.03.004.

[17] K. Huang, W. Su, X.C. Zhang, C.A. Chen, S. Zhao, X.Y. Yan, J. Jiang, T.H. Zhu, J. Z. Zhao, Cowpea-like bi-lineage nanofiber mat for repairing chronic rotator cuff tear and inhibiting fatty infiltration, Chem. Eng. J. 392 (2020), 123671, https://doi.org/10.1016/j.cej.2019.123671.

[18] B.J. Chen, Y.P. Liang, L. Bai, M.G. Xu, J. Zhang, B.L. Guo, Z.H. Yin, Sustained release of magnesium ions mediated by injectable self-healing adhesive hydrogel promotes fibrocartilaginous interface regeneration in the rabbit rotator cuff tear model, Chem. Eng. J. 396 (2020), 125335, https://doi.org/10.1016/j.cej.2020.125335.

[19] A. Sensini, G. Massafra, C. Gotti, A. Zucchelli, L. Cristofolini, Tissue engineering for the insertions of tendons and ligaments: an overview of electrospun biomaterials and structures, Front. Bioeng. Biotechnol. 9 (2021), 645544, https://doi.org/10.3389/fbioe.2021.645544.

[20] A. Sensini, L. Cristofolini, T Biofabrication of electrospun scaffolds for the regeneration of tendons and ligaments, Materials 11 (10) (2018) 1963, https://doi.org/10.3390/ma11101963.

[21] S. Ruiz-Alonso, M. Lafuente-Merchan, J. Ciriza, L. Saenz-del-Burgo, J.L. Pedraz, Tendon tissue engineering: cells, growth factors, scaffolds and production techniques, J. Contr. Release 333 (2021) 448–486, https://doi.org/10.1016/j.jconrel.2021.03.040.

[22] H.C. Quan, W. Yang, M. Lapeyriere, E. Schaible, R.O. Ritchie, M.A. Meyers, Structure and mechanical adaptability of a modern elasmoid fish scale from the common carp, Matter 3 (3) (2020) 842–863, https://doi.org/10.1016/j.matt.2020.05.011.

[23] W. Yang, H.C. Quan, M.A. Meyers, R.O. Ritchie, Arapaima fish scale: one of the toughest flexible biological materials, Matter 1 (6) (2019) 1557–1566, https://doi.org/10.1016/j.matt.2019.09.014.

[24] S. Gil-Duran, D. Arola, E.A. Ossa, Effect of chemical composition and microstructure on the mechanical behavior of fish scales from Megalops Atlanticus, J. Mech. Behav. Biomed. Mater. 56 (2016) 134–145, https://doi.org/10.1016/j.jmbbm.2015.11.028.

[25] D. Arola, S. Murcia, M. Stossel, R. Pahuja, T. Linley, A. Devaraj, M. Ramulu, E. A. Ossa, J. Wang, The limiting layer of fish scales: structure and properties, Acta Biomater. 67 (2018) 319–330, https://doi.org/10.1016/j.actbio.2017.12.011.

[26] L. Salvatore, N. Gallo, M.L. Natali, L. Campa, P. Lunetti, M. Madaghiele, F.S. Blasi, A. Corallo, L. Capobianco, A. Sannino, Marine collagen and its derivatives: versatile and sustainable bio-resources for healthcare, Mater. Sci. Eng. C-Mater. Biol. Appl. 113 (2020), 110963, https://doi.org/10.1016/j.msec.2020.110963.

[27] C.D. Seaborn, F.H. Nielsen, Silicon deprivation decreases collagen formation in wounds and bone, and ornithine transaminase enzyme activity in liver, Biol. Trace Elem. Res. 89 (2002) 251–261, https://doi.org/10.1385/BTER:89:3:251.

[28] M.E. Wall, A.J. Banes, Early responses to mechanical load in tendon: role for calcium signaling, gap junctions and intercellular communication, J. Musculoskelet. Neuronal Interact. 5 (2005) 70–84.

[29] C.T. Wu, J. Chang, A review of bioactive silicate ceramics, Biomed. Mater. 8 (3) (2013), 032001, https://doi.org/10.1088/1748-6041/8/3/032001.

[30] J.X. Lu, M. Descamps, J. Dejou, G. Koubi, P. Hardouin, J. Lemaitre, J.P. Proust, The biodegradation mechanism of calcium phosphate biomaterials in bone, J. Biomed. Mater. Res. 63 (4) (2002) 408–412, https://doi.org/10.1002/jbm.10259.

[31] C. Yang, X.Y. Wang, B. Ma, H.B. Zhu, Z.G. Huan, N. Ma, C.T. Wu, J. Chang, 3D-printed bioactive Ca3SiO5 bone cement scaffolds with nano surface structure for bone regeneration, ACS Appl. Mater. Interfaces 9 (2017) 5757–5767, https://doi.org/10.1021/acsami.6b14297.

[32] V. Bunpetch, X.A. Zhang, T. Li, J.X. Lin, E.P. Maswikiti, Y. Wu, D.D. Cai, J. Li, S. F. Zhang, C.T. Wu, H.W. Ouyang, Silicate-based bioceramic scaffolds for dual-lineage regeneration of osteochondral defect, Biomaterials 192 (2019) 323–333, https://doi.org/10.1016/j.biomaterials.2018.11.025.

[33] L. Chen, C.J. Deng, J.Y. Li, Q.Q. Yao, J. Chang, L.M. Wang, C.T. Wu, 3D printing of a lithium-calcium-silicate crystal bioscaffold with dual bioactivities for osteochondral interface reconstruction, Biomaterials 196 (2019) 138–150, https://doi.org/10.1016/j.biomaterials.2018.04.005.

[34] X.Y. Wang, L. Gao, Y. Han, M. Xing, C.C. Zhao, J.L. Peng, J. Chang, Silicon-enhanced adipogenesis and angiogenesis for vascularized adipose tissue engineering, Adv. Sci. 5 (2018), 1800776, https://doi.org/10.1002/advs.201800776.

[35] X.T. Wang, L.Y. Wang, Q. Wu, F. Bao, H.T. Yang, X.Z. Qiu, J. Chang, Chitosan/calcium silicate cardiac patch stimulates cardiomyocyte activity and myocardial performance after infarction by synergistic effect of bioactive ions and aligned nanostructure, ACS Appl. Mater. Interfaces 11 (2019) 1449–1468, https://doi.org/10.1021/acsami.8b17754.

[36] W. Zhang, Z.L. Huang, S.S. Liao, F.Z. Cui, Nucleation sites of calcium phosphate crystals during collagen mineralization, J. Am. Ceram. Soc. 86 (2003) 1052–1054, https://doi.org/10.1111/j.1151-2916.2003.tb03422.x.

[37] P.U.P.A. Gilbert, M. Albrecht, B.H. Frazer, The organic-mineral interface in biominerals, Rev. Mineral. Geochem. 59 (2005) 157–185, https://doi.org/10.2138/rmg.2005.59.7.

[38] G.A. Johnson, D.M. Tramaglini, R.E. Levine, K. Ohno, N.Y. Choi, S.L.Y. Woo, Tensile and viscoelastic properties of human patellar tendon, J. Orthop. Res. 12 (1994) 796–803, https://doi.org/10.1002/jor.1100120607.

[39] S.D. Rawson, L. Margetts, J.K.F. Wong, S.H. Cartmell, Sutured tendon repair; a multi-scale finite element model, Biomech. Model. Mechanobiol. 14 (2015) 123–133, https://doi.org/10.1007/s10237-014-0593-5.

[40] D. Liu, C. Yi, C.C. Fong, Q. Jin, Z. Wang, W.K. Yu, D. Sun, J. Zhao, M. Yang, Activation of multiple signaling pathways during the differentiation of mesenchymal stem cells cultured in a silicon nanowire microenvironment, Nanomed. Nanotechnol. Biol. Med. 10 (6) (2014) 1153–1163, https://doi.org/10.1016/j.nano.2014.02.003.

[41] A.M.C. Barradas, H.A.M. Fernandes, N. Groen, Y.C. Chai, J. Schrooten, J. van de Peppel, J.P.T.M. van Leeuwen, C.A. van Blitterswijk, J. de Boer, A calcium-induced signaling cascade leading to osteogenic differentiation of human bone marrow-derived mesenchymal stromal cells, Biomaterials 33 (2012) 3205–3215, https://doi.org/10.1016/j.biomaterials.2012.01.020.

[42] M. Shi, Y. Zhou, J. Shao, Z. Chen, B. Song, J. Chang, C. Wu, Y. Xiao, Stimulation of osteogenesis and angiogenesis of hBMSCs by delivering Si ions and functional drug from mesoporous silica nanospheres, Acta Biomater. 21 (2015) 178–189, https://doi.org/10.1016/j.actbio.2015.04.019.

[43] A. Gereli, U. Akgun, S. Uslu, I. Agir, F. Ates, U. Nalbantoglu, The effect of organic silicon injection on Achilles tendon healing in rats, Acta Orthop. Traumatol. Turcica 48 (2014) 346–354, https://doi.org/10.3944/AOTT.2014.3162.

[44] D. Zhai, M.C. Xu, L.Q. Liu, J. Chang, C.T. Wu, Silicate-based bioceramics regulating osteoblast differentiation through a BMP2 signalling pathway, J. Mater. Chem. B 5 (35) (2017) 7297–7306, https://doi.org/10.1039/c7tb01931a.

[45] X.X. Dong, X.Y. Wang, M. Xing, C.C. Zhao, B. Guo, J.K. Cao, J. Chang, Inhibition of the negative effect of high glucose on osteogenic differentiation of bone marrow stromal cells by silicon ions from calcium silicate bioceramics, Regen. Biomater. 7 (1) (2020) 9–18, https://doi.org/10.1093/rb/rbz030.

[46] L. Rossetti, L.A. Kuntz, E. Kunold, J. Schock, K.W. Muller, H. Grabmayr, J. Stolberg-Stolberg, F. Pfeiffer, S.A. Sieber, R. Burgkart, A.R. Bausch, The microstructure and micromechanics of the tendon-bone insertion, Nat. Mater. 16 (2017) 664–670, https://doi.org/10.1038/NMAT4863.

[47] K. Atesok, F.H. Fu, M.R. Wolf, M. Ochi, L.M. Jazrawi, M.N. Doral, J.H. Lubowitz, S. A. Rodeo, Augmentation of tendon-to-bone healing, J. Bone Joint Surg.-Am. 96A (2014) 513–521, https://doi.org/10.2106/JBJS.M.00009.

[48] M.A. Zumstein, A. Ladermann, S. Raniga, M.O. Schar, The biology of rotator cuff healing, Orthop. Traumatol.-Surg. Res. 103 (2017) S1–S10, https://doi.org/10.1016/j.otsr.2016.11.003.

[49] R.M.A. Domingues, S. Chiera, P. Gershovich, A. Motta, R.L. Reis, M.E. Gomes, Enhancing the biomechanical performance of anisotropic nanofibrous scaffolds in tendon tissue engineering: reinforcement with cellulose nanocrystals, Adv. Healthc. Mater. 5 (2016) 1364–1375, https://doi.org/10.1002/adhm.201501048.
[50] A. Inui, T. Kokubu, Y. Mifune, R. Sakata, H. Nishimoto, K. Nishida, T. Akisue, R. Kuroda, M. Satake, H. Kaneko, H. Fujioka, Regeneration of rotator cuff tear using electrospun poly(d,l-lactide-co-glycolide) scaffolds in a rabbit model, Arthroscopy 28 (12) (2012) 1790–1799, https://doi.org/10.1002/10.1016/j.arthro.2012.05.887.
[51] X. He, Y. Li, J.X. Guo, J.K. Xu, H.Y. Zu, L. Huang, M.T.Y. Ong, P.S.H. Yung, L. Qin, Biomaterials developed for facilitating healing outcome after anterior cruciate ligament reconstruction: efficacy, surgical protocols, and assessments using preclinical animal models, Biomaterials 269 (2021), 120625, https://doi.org/10.1016/j.biomaterials.2020.120625.
[52] T.Y. Lei, T. Zhang, W. Ju, X. Chen, B.C. Heng, W.L. Shen, Z. Yin, Biomimetic strategies for tendon/ligament-to-bone interface regeneration, Bioact. Mater. 6 (8) (2021) 2491–2510, https://doi.org/10.1016/j.bioactmat.2021.01.022.
[53] Y.C. Sun, H.W. Jung, J.M. Kwak, J. Tan, Z. Wang, I.H. Jeon, Reconstruction of large chronic rotator cuff tear can benefit from the bone-tendon composite autograft to restore the native bone-tendon interface, J. Orthop. Transl. 24 (2020) 175–182, https://doi.org/10.1016/j.jot.2020.01.001.
[54] Y.C. Zhou, S.S. Xie, Y.F. Tang, X.N. Li, Y. Cao, J.Z. Hu, H.B. Lu, Effect of book-shaped acellular tendon scaffold with bone marrow mesenchymal stem cells sheets on bone - tendon interface healing, J. Orthop. Transl. 26 (2021) 162–170, https://doi.org/10.1016/j.bioactmat.2021.01.022.
[55] C. Chen, F. Liu, Y. Tang, J. Qu, Y. Cao, C. Zheng, Y. Chen, M. Li, C. Zhao, L. Sun, J. Hu, H. Lu, Book-shaped acellular fibrocartilage scaffold with cell-loading capability and chondrogenic inducibility for tissue-engineered fibrocartilage and bone-tendon healing, ACS Appl. Mater. Interfaces 11 (2019) 2891–2907, https://doi.org/10.1021/acsami.8b20563.
[56] Z. Yin, X. Chen, H.X. Song, J.J. Hu, Q.M. Tang, T. Zhu, W.L. Shen, J.L. Chen, H. Liu, B.C. Heng, H.W. Ouyang, Electrospun scaffolds for multiple tissues regeneration in vivo through topography dependent induction of lineage specific differentiation, Biomaterials 44 (2015) 173–185, https://doi.org/10.1016/j.biomaterials.2014.12.027.
[57] S. Samavedi, P. Vaidya, P. Gaddam, A.R. Whittington, A.S. Goldstein, Electrospun meshes possessing region-wise differences in fiber orientation, diameter, chemistry and mechanical properties for engineering bone-ligament-bone tissues, Biotechnol. Bioeng. 111 (2014) 2549–2559, https://doi.org/10.1002/bit.25299.
[58] S. Tarafder, J.A. Brito, S. Minhas, L. Effiong, S. Thomopoulos, C.H. Lee, In situ tissue engineering of the tendon-to-bone interface by endogenous stem/progenitor cells, Biofabrication 12 (2019), 015008, https://doi.org/10.1088/1758-5090/ab48ca.
[59] Y. Cao, S.B. Yang, D.Y. Zhao, Y. Li, S.S. Cheong, D. Han, Q.F. Li, Three-dimensional printed multiphasic scaffolds with stratified cell-laden gelatin methacrylate hydrogels for biomimetic tendon-to-bone interface engineering, J. Orthop. Transl. 23 (2020) 89–100, https://doi.org/10.1016/j.jot.2020.01.004.
[60] I.E. Wang, D.R. Bogdanowicz, S. Mitroo, J. Shan, S. Kala, H.H. Lu, Cellular interactions regulate stem cell differentiation in tri-culture, Connect. Tissue Res. 57 (2016) 476–487, https://doi.org/10.1080/03008207.2016.1230106.
[61] M. Meyers, J. McKittrick, P. Chen, Structural biological materials: critical mechanics-materials connections, Science 339 (2013) 773–779, https://doi.org/10.1126/science.1220854.
[62] Y.Q. Zhou, J.Y. Zhang, H.S. Wu, M.V. Hogan, J.H.C. Wang, The differential effects of leukocyte-containing and pure platelet-rich plasma (PRP) on tendon stem/progenitor cells - implications of PRP application for the clinical treatment of tendon injuries, Stem Cell Res. Ther. 6 (2015), https://doi.org/10.1186/s13287-015-0172-4.
[63] S.A. Shah, I. Kormpakis, N. Havlioglu, M.S. Ominsky, L.M. Galatz, S. Thomopoulos, Sclerostin antibody treatment enhances rotator cuff tendon-to-bone healing in an animal model, J. Bone Joint Surg.-Am. 99 (2017) 855–864, https://doi.org/10.2106/JBJS.16.01019.
[64] C. Zhang, H. Yuan, H. Liu, X. Chen, P. Lu, T. Zhu, L. Yang, Z. Yin, B.C. Heng, Y. Zhang, H.W. Ouyang, Well-aligned chitosan-based ultrafine fibers committed teno-lineage differentiation of human induced pluripotent stem cells for Achilles tendon regeneration, Biomaterials 53 (2015) 716–730, https://doi.org/10.1016/j.biomaterials.2015.02.051.
[65] Z. Yin, X. Chen, J.L. Chen, W.L. Shen, T.M. Hieu Nguyen, L. Gao, H.W. Ouyang, The regulation of tendon stem cell differentiation by the alignment of nanofibers, Biomaterials 31 (2010) 2163–2175, https://doi.org/10.1016/j.biomaterials.2009.11.083.
[66] M. Younesi, A. Islam, V. Kishore, J.M. Anderson, O. Akkus, Tenogenic induction of human mscs by anisotropically aligned collagen biotextiles, Adv. Funct. Mater. 24 (2014) 5762–5770, https://doi.org/10.1002/adfm.201400828.
[67] S. Choi, Y. Choi, J. Kim, Anisotropic hybrid hydrogels with superior mechanical properties reminiscent of tendons or ligaments, Adv. Funct. Mater. 29 (2019), 1904342, https://doi.org/10.1002/adfm.201904342.
[68] Y.J. No, S. Tarafder, B. Reischl, Y. Ramaswamy, C. Dunstan, O. Friedrich, C.H. Lee, H. Zreiqat, High-strength fiber-reinforced composite hydrogel scaffolds as biosynthetic tendon graft material, ACS Biomater. Sci. Eng. 6 (2020) 1887–1898, https://doi.org/10.1021/acsbiomaterials.9b01716.
[69] M. Laranjeira, R.M.A. Domingues, R. Costa-Almeida, R.L. Reis, M.E. Gomes, 3D mimicry of native-tissue-fiber architecture guides tendon-derived cells and adipose stem cells into artificial tendon constructs, Small 13 (2017), 1700689, https://doi.org/10.1002/smll.201700689.
[70] E. Gentleman, A.N. Lay, D.A. Dickerson, E.A. Nauman, G.A. Livesay, K.C. Dee, Mechanical characterization of collagen fibers and scaffolds for tissue engineering, Biomaterials 24 (2003) 3805–3813, https://doi.org/10.1016/S0142-9612(03)00206-0.
[71] M.T.I. Mredha, Y.Z. Guo, T. Nonoyama, T. Nakajima, T. Kurokawa, J.P. Gong, A facile method to fabricate anisotropic hydrogels with perfectly aligned hierarchical fibrous structures, Adv. Mater. 30 (2018), 1704937, https://doi.org/10.1002/adma.201704937.
[72] B. Aghaei-Ghareh-Bolagh, S.M. Mithieux, M.A. Hiob, Y. Wang, A. Chong, A. S. Weiss, Fabricated tropoelastin-silk yarns and woven textiles for diverse tissue engineering applications, Acta Biomater. 91 (2019) 112–122, https://doi.org/10.1016/j.actbio.2019.04.029.
[73] Z. Wang, W.J. Lee, B.T.H. Koh, M. Hong, W. Wang, P.N. Lim, J. Feng, L.S. Park, M. Kim, E.S. Thian, Functional regeneration of tendons using scaffolds with physical anisotropy engineered via microarchitectural manipulation, Sci. Adv. 4 (10) (2018), https://doi.org/10.1126/sciadv.aat4537 eaat4537.
[74] D. Sheng, J. Li, C. Ai, S. Feng, T. Ying, X. Liu, J. Cai, X. Ding, W. Jin, H. Xu, J. Chen, S. Chen, Electrospun PCL/Gel-aligned scaffolds enhance the biomechanical strength in tendon repair, J. Mat. Chem. B 7 (2019) 4801–4810, https://doi.org/10.1039/c9tb00837c.